

# Numerical Analysis of Flow Characteristics around Circular Cylinders with Arc Grooves

by

Shinichi Takayama<sup>\*1</sup> and Katsumi Aoki<sup>\*2</sup>

(received on March 31, 2005 & accepted on October 18, 2005)

## Abstract

In this study, the drag reduction by arc grooves on a circular cylinder is investigated. Thirty-two arc grooves are formed on the cylinder surface, and three cylinders with different arc groove depths are used. The critical Reynolds numbers of the circular cylinders with grooves are smaller than that of a smooth cylinder. The flow characteristics around the circular cylinders with grooves are numerically analyzed using the Reynolds number  $Re=1.2 \times 10^5$ . The results of this numerical analysis revealed that separation bubbles are generated inside the grooves. The separation bubbles transform a laminar boundary layer into a turbulent boundary layer. Therefore, the drag coefficients of circular cylinders with grooves are smaller than that of the smooth cylinder.

**Keywords:** Numerical analysis, Circular cylinder, Fluid force, Separation, Grooves

## 1. Introduction

Various studies on drag and lift of a circular cylinder set in a uniform flow have been reported. In the case of a stationary smooth cylinder, the drag coefficient shows a characteristic change with Reynolds number. In general, the drag coefficient of a smooth cylinder passes through three regions (subcritical, critical and supercritical regions) as Reynolds number increases. The critical Reynolds number of a smooth cylinder is  $Re=3.5 \times 10^5$ . The drag coefficient characteristics for the surface structure of circular cylinders is described by Achenbach<sup>(1)</sup> and Achenbach

and Heinecke<sup>(2)</sup>. As the roughness of the circular cylinder surface increases, the critical point shifts to the low Reynolds number side, and the drag coefficient of a rough cylinder becomes smaller than that of a smooth cylinder. However, as Reynolds number increases further, the drag coefficient of rough cylinders increases. Aoki and coworkers<sup>(3), (4)</sup> reported on cylinders with grooves (regular roughness), where the critical Reynolds number was smaller than that for a circular cylinder without grooves. However, the investigation of the drag reduction mechanism for a cylinder with grooves has not yet been carried out and the details of flow around a cylinder with grooves are not yet investigated for the supercritical

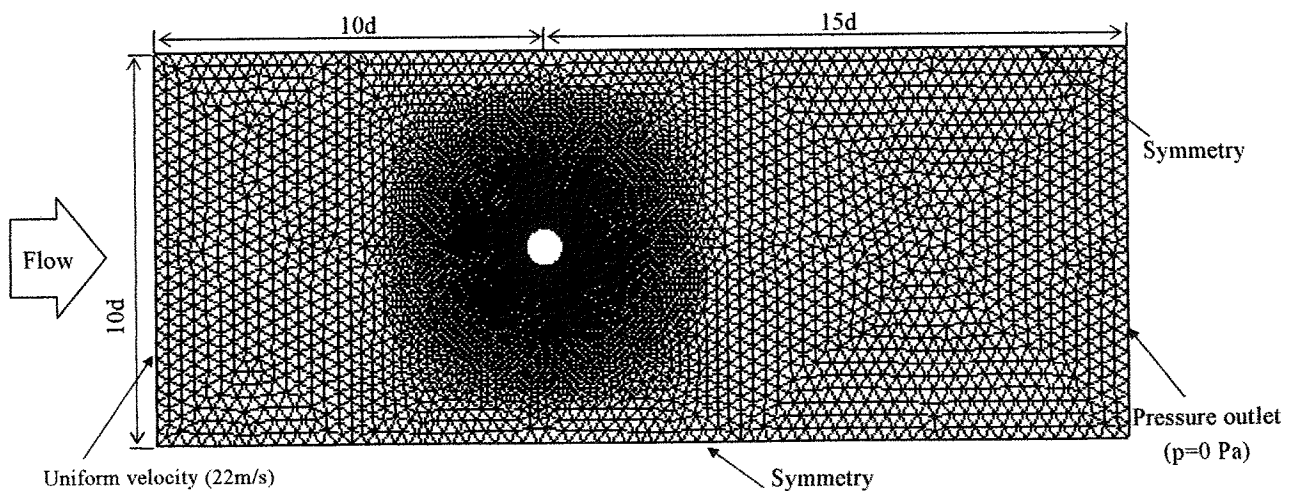


Fig. 1 Calculation area and boundary conditions

\* 1 Graduate Student, Course of Mechanical Engineering  
\* 2 Professor, Department of Mechanical Engineering

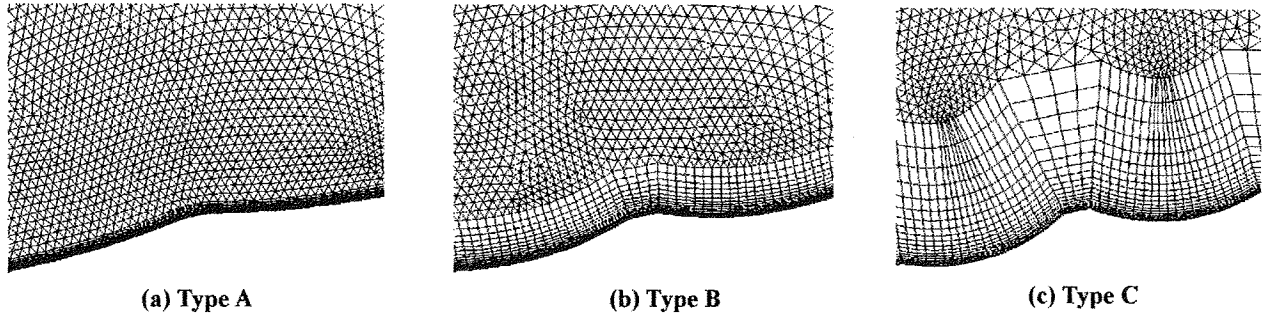
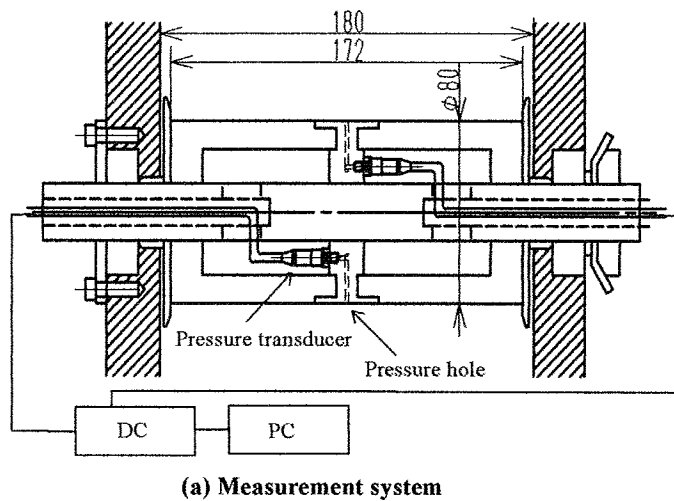
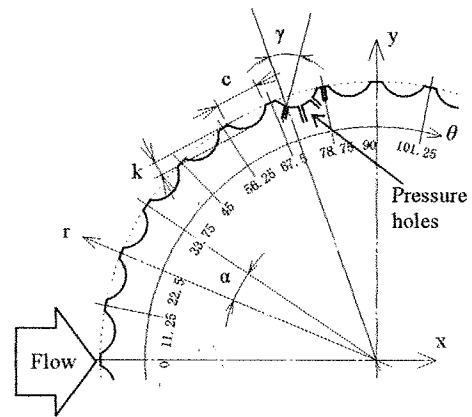


Fig. 2 Mesh near the surface



(a) Measurement system



(b) Cross section of cylinder with grooves

Fig. 3 Experimental setup for measuring surface pressure

Table 1 Specifications of cylinder with grooves

Type	A	B	C
k (mm)	0.30	0.58	0.94
d (mm)	80		
c (mm)	6.76		
$\alpha$ (deg)	11.25		
$k/d (\times 10^{-3})$	3.75	7.25	11.75

region. The final purpose of this study is to clarify the mechanism of the drag reduction for the cylinder with grooves. In this study, the flow characteristics of a surface-grooved cylinder are clarified by numerical analysis for the supercritical region.

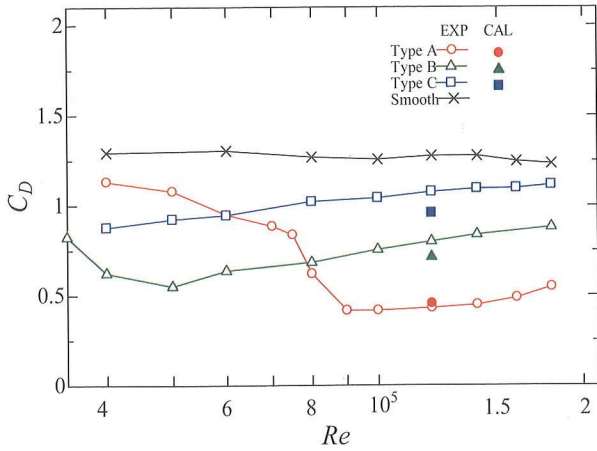
## 2. Numerical analysis

For the calculation, the general heat and fluid software Fluent was used. Figure 1 shows the area and boundary conditions of the numerical analysis. The test cylinder diameter is  $d=80\text{mm}$  and the area of analysis is 2 dimensional ( $25d$  length,  $10d$  wide). The cylinder set at  $10d$  from the line of the velocity inlet. The number of mesh elements is about 400,000, and in the calculation of the boundary layer, a low-Reynolds number model was used because of the wall function is not very accurate near the separation point. Thirty-two arc grooves are formed on the surface of three cylinders with three groove depths of 0.3mm (Type A), 0.58mm (Type B), and

0.94mm (Type C). Figure 2 shows the mesh near the surface of the cylinders with grooves. The realizable k- $\epsilon$  model is used as the turbulence model.

## 3. Experimental apparatus

The experiments are conducted in a wind tunnel 380mm high and 180mm wide. The air velocity used is 7 to 35m/s ( $Re=0.4 \times 10^5 \sim 1.8 \times 10^5$ ), and the turbulence level is about 0.6% in the wind velocity range used. The diameter of the test cylinder is 80mm and the length is 172mm. Side plates of 110mm diameter are installed at the cylinder end to prevent secondary flow. The cross section and the specifications of the cylinders are shown in Figures 3 (a) and (b) and Table 2, respectively. Thirty-two arc grooves are formed parallel to the axis on each cylinder. Three pressure holes of 0.8mm diameter are set inside the grooves and one is set outside. This pressure hole is set perpendicular to the groove surface at


**Fig. 4 Drag coefficient**

one-quarter of the angle made by each pair of adjoined swells. The pressure transducer is connected to each pressure hole and pressure on the cylinder surface is measured. The output signal from the pressure transducer is read on a computer after passing through a DC amplifier.

## 4. Results and discussion

### 4.1 Drag coefficient

Figure 4 shows the drag coefficient plotted against the Reynolds number. In the experiment, drag is calculated from the pressure distribution on the cylinder surface and the drag coefficient  $C_D$  is calculated using the following equation.

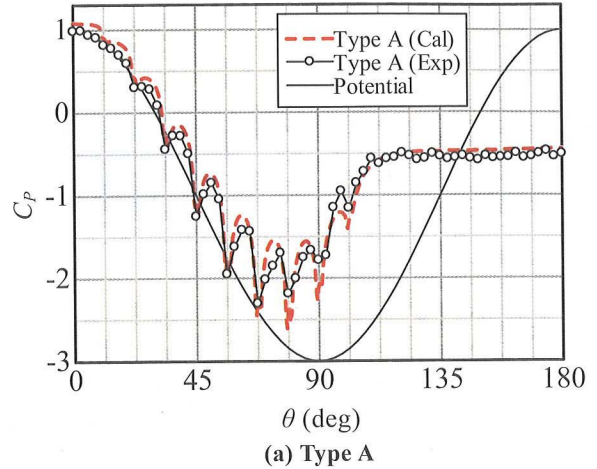
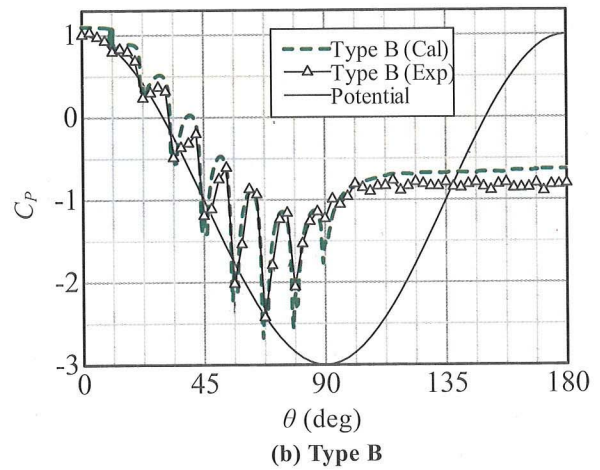
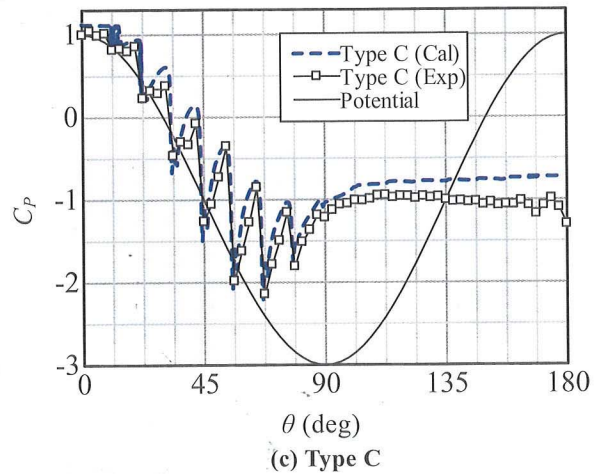
$$C_D = \frac{D}{\rho U^2 d l} \quad (1)$$

$D$ : drag,  $\rho$ : density of air,  $U$ : uniform flow,  $d$ : diameter of cylinder  
 The drag is calculated by integrating the pressure distribution and the axial direction was decided the unit length. The pressure distribution is measured in state of the stagnation point being outside of the grooves. The drag coefficient of the smooth cylinder is constant with changing Reynolds number because it is in the subcritical region. The drag coefficient of a cylinder with grooves increases gradually after an initial decrease. However, the drag coefficient of the Type C cylinder shows a tendency to only increase gradually. The drag coefficient decreases in the critical region, and increases gradually in the supercritical region. As groove depth increases, the critical region shifts to lower Reynolds number. The drag coefficient of the Type A cylinder is smaller than those of the other cylinders with grooves in the supercritical region. Also, the drag coefficient increases as the grooves become deeper. In the supercritical region, the drag coefficients determined experimentally and by numerical analysis approximately agree.

### 4.2 Pressure distribution

Figure 5 shows the pressure distribution at  $Re=1.2 \times 10^5$ . The pressure coefficient  $C_P$  is expressed as

$$C_P = \frac{P - P_0}{\rho U^2 / 2} \quad (2)$$


**(a) Type A**

**(b) Type B**

**(c) Type C**
**Fig. 5 Pressure distribution ( $Re=1.2 \times 10^5$ )**

$P$ : surface pressure,  $P_0$ : static pressure of uniform flow.

The pressure distribution obtained by the experiment is similar to the numerical analysis results. In the experimental results for the Type A cylinder, the pressures at the bottom of grooves were the highest at 56.25deg from the stagnation point, and the pressures on the downstream side of the groove were the highest beyond 56.25 deg. For Type B and Type C cylinders, the pressures on the downstream side of the groove were the highest beyond 22.5deg.

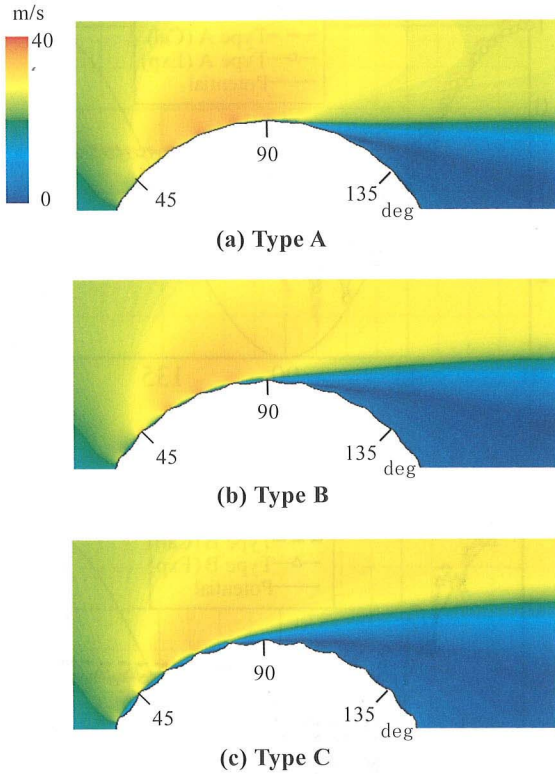


Fig. 6 Contours of velocity magnitude ( $Re=1.2 \times 10^5$ )

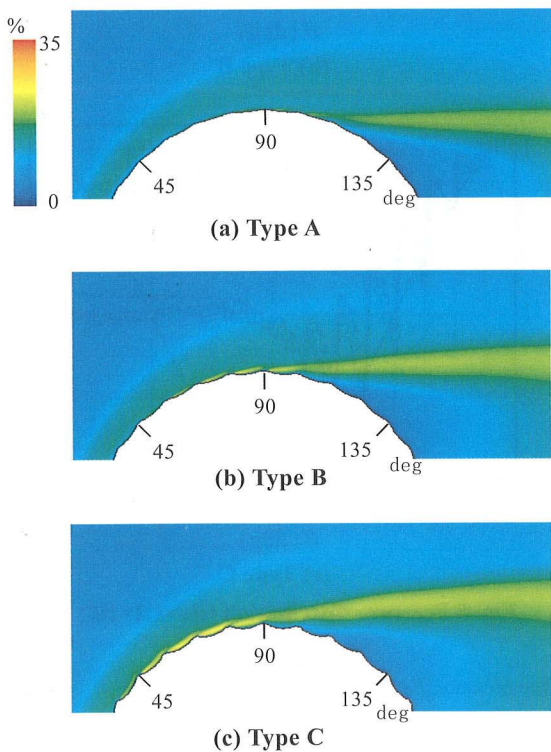


Fig. 7 Contours of turbulence intensity ( $Re=1.2 \times 10^5$ )

**4.3 Velocity and turbulence intensity around cylinder with grooves**

Figure 6 shows the contours of velocity magnitude around the cylinders with grooves at  $Re=1.2 \times 10^5$  (supercritical region). As grooves become deeper, the velocity around the cylinder decreases

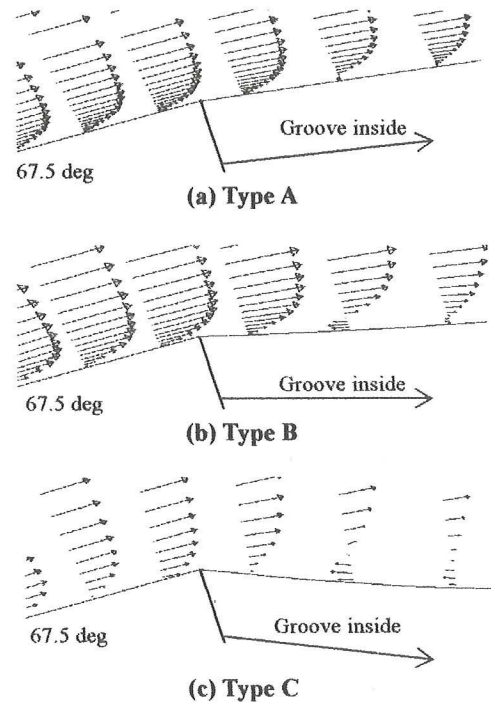


Fig. 8 Velocity vectors near 67.5 deg ( $Re=1.2 \times 10^5$ )

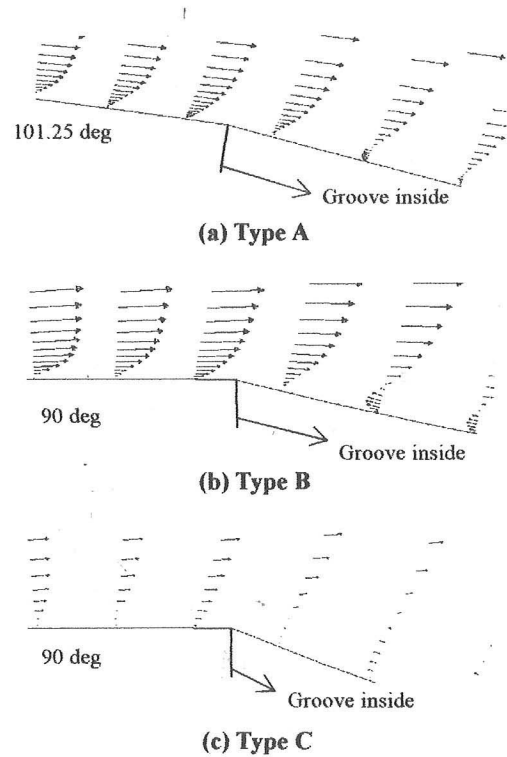
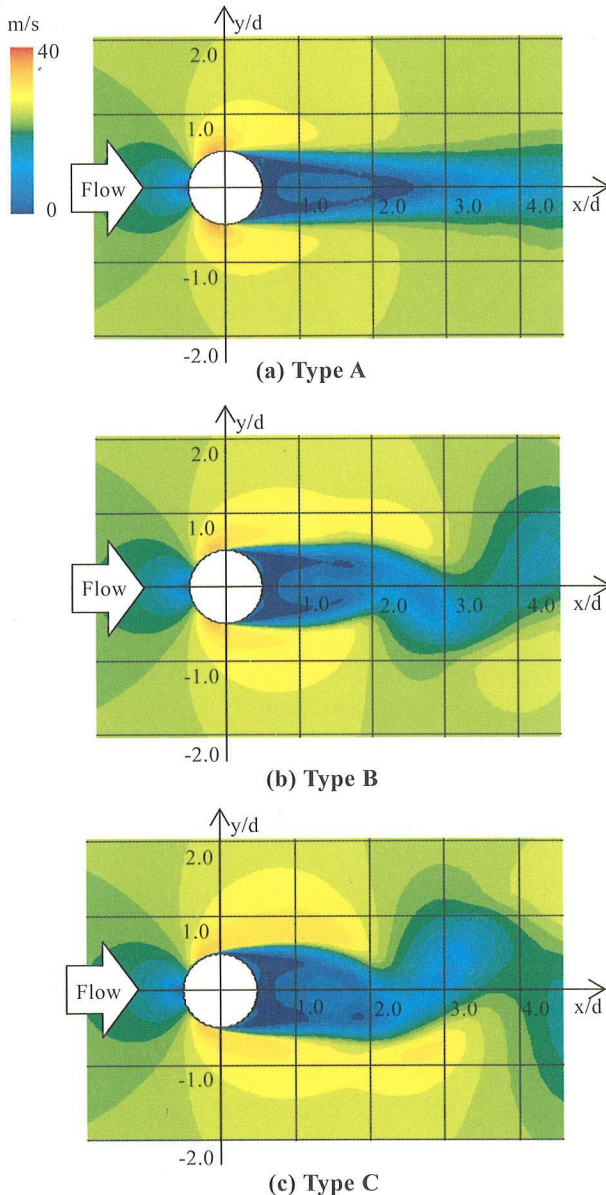


Fig. 9 Velocity vectors near separation point ( $Re=1.2 \times 10^5$ )

and the separation point shifts to the upstream side. However, the separation point for Type B and Type C cylinders is the same, at 90 deg. For the smooth cylinder, the separation point is at about 80 deg at  $Re=1.2 \times 10^5$  (subcritical region) in general and the boundary layer is laminar.

Figure 7 shows the contours of turbulence intensity around the



**Fig. 10** Contours of velocity around cylinders with grooves ( $Re=1.2 \times 10^5$ , Unsteady)

cylinders with grooves. As grooves depth increases, the turbulence intensity in the grooves increases. It is thought that the turbulent intensity in the grooves changes the boundary layer from laminar to turbulent.

#### 4.3 Velocity distribution near the surface and wake

Figure 8 shows the velocity vectors near 67.5 deg. The flow separated outside the groove and reattached inside the groove. Therefore, a vortex (separation bubble) occurs inside the groove. As a result, the pressure coefficient on the downstream side of grooves is the highest, and the turbulence intensity in the groove increases. It is thought that the separation bubble assisted the change of the boundary layer to turbulent flow from laminar flow.

Figure 9 shows the velocity vectors near the separation point at  $Re = 1.2 \times 10^5$ . The separation point is at 101.25deg for the Type A cylinder and 90 deg for Type B and Type C cylinders. The separation

point shifts upstream as groove depth increases, and it is thought that the separation point then occurs only outside the grooves. The separation points of Type B and Type C cylinders are at the same angle, however, their drag coefficients are different. In general, the separation point of a smooth cylinder is at about 80 deg at  $Re = 1.2 \times 10^5$  (subcritical region). However, for cylinders with grooves, the separation point shifts downstream because the boundary layer has a turbulent flow.

Figure 10 shows the contours of velocity magnitude around cylinders with grooves at  $Re = 1.2 \times 10^5$  for the unsteady condition. The size of the wake for Type B and Type C cylinders is different, though the separation point is at the same angle. Therefore, the drag coefficients of Type B and Type C cylinders differ.

## 5. Conclusions

The following results were obtained by the numerical analysis and experiment using three kinds of cylinders with different groove depths.

1. A subcritical, a critical, and a supercritical region exist for the cylinder with grooves as well as for a smooth cylinder. The critical region moves to a lower Reynolds number as the grooves become deeper, and the minimum  $C_D$  value for a cylinder with deep grooves is larger than that for the cylinder with shallow grooves.
2. The separation bubbles that form inside the groove assist the change of the boundary layer from laminar flow to turbulent flow and then the separation point shifts downstream, in comparison with that of a smooth cylinder. Therefore, the drag coefficient of a cylinder with grooves is smaller than that of a smooth cylinder.
3. As grooves become deeper, the separation point moves upstream. However, the separation point is affected by the groove position.
4. Even if the separation point is the same, the velocity around a cylinder with grooves and the size of the wake are different. Therefore, the drag coefficient is different in the supercritical region.

## References

1. E. Achenbach, Influence of surface roughness on the cross-flow around a circular cylinder, *J. Fluid Mech.*, Vol. 46, No 2, pp 321-335, 1971
2. E. Achenbach and E. Heinecke, On vortex shedding from smooth and rough cylinders in the range of Reynolds number  $6 \times 10^3$  to  $5 \times 10^6$ , *J. Fluid Mech.*, Vol. 109, pp 239-251, 1981
3. K. Aoki, T. Shimada and S. Takayama, Flow characteristics around circular cylinder with arc grooves, *Proc 7<sup>th</sup> Asian Symposium on Visualization*, Singapore, 2003
4. Y. Wakai, S. Takayama and K. Aoki, Effect of drag reduction for surface structure of circular cylinder, *Proc 11<sup>th</sup> International Symposium on Flow Visualization*, U.S.A., 2004